The two-way bridge between transition lifetimes and dipole polarizability: A case study of Mg-like P (IV)

Nicholas Reshetnikov[1] and Lorenzo J. Curtis[2]

[1]Physics Department, Harvard University, Cambridge MA 02138
[2]Department of Physics and Astronomy, University of Toledo, Toledo Ohio 43606

Abstract

For atoms and ions with the ground state electron configuration of ns^2 $^1S_0$, a remarkable approximation of the dipole polarizability can be made from just *one* transition lifetime measurement. Particularly, since the ns^2 $^1S_0 - nsnp$ $^1P_1^\circ$ intrashell transition dominates the total oscillator strength of transitions to the ground state, it in turn dominates the dipole polarizability of the ion. The oscillator strength serves as the quantum mechanical link between the two empirical quantities, allowing knowledge of both from a precise measurement of one. This relationship is especially useful for studying atoms for which precise measurements of either the lifetime or dipole polarizability are difficult or impossible to make. What is more, with just a few such precise measurements of either quantity, isoelectronic linearities can be exploited to interpolate to ions beyond empirical study. The Mg-like P (IV) ion, with two old and conflicting lifetime measurements and one precise dipole polarizability measurement, gave an excellent opportunity to test the two-way relationship. However, difficulty caused by cascading from higher energy states and blending from higher charged ions made the lifetime measure of .35(2) ns an unsatisfactory upper limit. If the blending can be removed by running the phosphorus beam at lower energies, the ANDC method can be used to decouple the cascades. Whether or not this attempt succeeds, the problems in precise lifetime determination of P (IV) underscore the usefulness of the two-way lifetime-dipole polarizability bridge and isoelectronic interpolation to sidestep empirical constraints on precise measurement.

1 August 2007

Introduction / Background

Given the remarkably large number of phenomena that can be explained solely through valence shell electron interactions, little attention has been paid to the rest of the electrons, hidden in the "fuzzy" inner electrons clouds. Add to this the high energy needed to liberate those electrons and the difficulty in isolating them, and it is understandable why there has been such limited research in the area. Nonetheless, there are ways to get at the inner shells without the complications arising from the outer electrons. Ionizing atoms is one of the best ways of doing just this—peeling off the outer electrons to reveal the once-hidden electron layers underneath. In other words, a system considered beyond modern experimentation techniques can be effectively studied by transforming it into a more familiar one with valence electrons.

A very important property that can be studied in such a system is the dipole polarizability α_d, effectively a measure of an atom's tendency to form a dipole in an electric field. While it may seem like an obscure quantity, the dipole polarizability is really a fundamental property of the quantum mechanics of the electron. Additionally, it is responsible for a number of practical physical phenomena ranging from dielectrics to indexes of refraction and intermolecular forces.

However, direct measurements of the dipole polarizability require very complex equipment and procedures. It is simpler to determine α_d indirectly, through measurements of transition lifetimes of highly excited states of the ion. These measurements allow a direct calculation of the quantum mechanical quantity called the oscillator strength f – an analog of the spring constant for simple harmonic oscillators. With knowledge of the energy and oscillator strength of each transition to the ground state of the ion, α_d can be calculated. Unfortunately, gathering such data is not very feasible given the theoretical infinite number of energy states and oscillator strengths to take into account. But it turns out that for atoms with the outer electron configuration of ns^2—that is, two electrons in the outer-shell (i.e. Mg, Cd, Zn, etc.)—a remarkably accurate approximation of α_d can be made with just *one* precise lifetime measurement [1].

For atoms with this electron configuration the transition that dominates the oscillator strength—and equivalently the dipole polarizability—has three important properties. It is (1) the lowest resonance energy transition to the ground state of the valence shell, (2) an unbranched transition—the only one that goes directly to the ground state, and (3) an *intra*-shell transition, between the s (ground) and p states of the valence energy level. It is intuitively plausible that a transition closest to the ion nucleus (lowest resonance), with no interference from other possible transitions (unbranched) would be a substantial part of the total oscillator strength of the ion. Yet, it is remarkable the overwhelming extent to which this one transition dominates the total sum of the transition oscillator strengths. A rigorous explanation for this domination involves cancellation in the dipole transition matrix for particular energy levels, and is described in detail by Curtis in *Atomic Structures and Lifetimes* [2].

Unfortunately, this approach of deducing α_d from lifetime measurements is essentially limited to ions with ns and ns^2 electron configurations. Further, even for ions with favorable configurations, very high energies are required to sufficiently ionize the atoms to get at the very deep electrons. Once again one can use an indirect method to get around this practical constraint. Through another quantum mechanical quantity called the line strength S, a linear,

regularly varying plot can be made of isolectronic sequences of ions. Because of their linearity, these plots allow for interpolation and extrapolation to highly ionized atoms (both positive and negative) based on a just a few precise, moderately-ionized lifetime measurements. Further, they encode information on not just the lifetime, but also the oscillator strengths. There is thus the potential for compiling databases of dipole polarizabilities and transition lifetimes from any given one of these values. A simple schematic representation of the relationships is shown below in Figure 1.

Figure 1: Relationship between important quantities derived from lifetime measurements of the lowest level intrashell transition to the ground state of simple ions
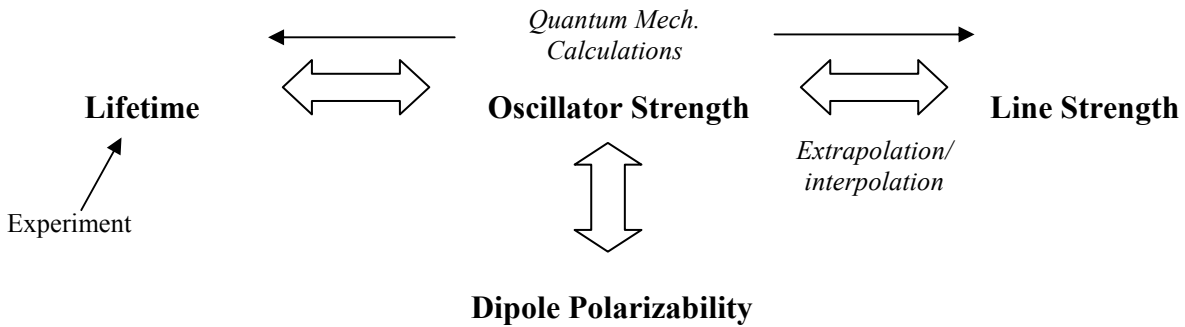
Theory

Now while the theoretical formulation of these quantities is steeped in quantum mechanics, it is helpful to see the relationships between the different quantities mathematically. These relationships are formulated by Curtis in [1].

The inverse correlation between the lifetime τ and the oscillator strength f of a $ns^2 - nsnp$ transition is given by

$$\frac{1}{\tau_{np}} = \frac{2\,c\,\alpha^4}{3\,a_0} E_{ns,np}^2 \; f_{ns,np} \tag{1}$$

where α is the fine structure constant and a_0 is the Bohr radius. The *ns np* simply signifies the intrashell transition from the *p* to the *s* (ground state) orbital. Intuitively, this inverse relationship makes sense when the *f* is compared to the spring constant. For just as a high spring constant means a stiffer oscillator with a higher frequency and more energy emission, so does a higher oscillator strength correspond to a faster release of energy in the transition—and thus a shorter lifetime.

The dipole polarizability for the ground state is directly proportional to the sum of the oscillator strengths:

$$\alpha_d = \sum_{n'} \frac{f_{ns,n'p}}{E_{ns,n'p}^2} \tag{2}$$

where *n'* is represents transitions from higher energy levels. Only the transitions to the ground state are considered as are relatively negligible.

Invoking the *f*-sum rule—that the sum of the oscillator strengths of every transition for a given ion is equal to its number of valence electrons N_e—we can formulate a good approximation of the dipole polarizability:

$$\alpha_d \approx \frac{f_{ns,np}}{E_{ns,np}^2} + \frac{N_e - f_{ns,np}}{2E_{ns,(n+1)p}^2} \tag{3}$$

The second term of the sum represents the uncertainty in the formulation, effectively taking the midpoint of the uncertainty range as an approximation for α_d. And for moderately ionized atoms this uncertainty is virtually negligible. Thus, a highly accurate approximation of the dipole polarizability can be made with knowledge of the dominant oscillator strength (derived from a single lifetime measurement using equation (1)).

The final piece in figure 1 is the line strength *S*, which is really the heart of the quantum mechanical formulation of the oscillator strength and in turn dipole polarizability. In Dirac notation it can be represented as,

$$S_{ns,np} = |\langle \psi_{ns} | r | \psi_{np} \rangle|^2 \tag{4}$$

where ψ represents the wave function for the given energy state, ns or np, of the ion. The relationship to the oscillator strength (and in turn through (3) to the dipole polarizability) is given by:

$$f_{ns,np} = \frac{2}{3} E_{ns,np} S_{ns,np} . \tag{5}$$

[1].

Experiment

Goal

The goal of the experiment was to improve the Mg isoelectronic plot of the line strength variation with atomic number by taking a lifetime measurement of the singlet $3s^2$ - 3s3p transition for P (IV). The interest in this lifetime comes from the fact that there are two earlier, incompatible measured lifetimes of .22 ns [3] and .35 ns [4]. Based on recent highly precise measurements of the dipole polarizability by Magnusson and Zetterberg [5], a very good estimate can be made of what the lifetime *should* be through equations (3) and (1). In fact, from the measured α_d, the theoretical lifetime should be ~.29 ns, right at the midpoint of the earlier two measurements! Beyond testing the validity of this theoretical coincidence, the new measurement would serve to not only improve the isolectronic plot, but also confirm the power of this translation between lifetimes and dipole polarizabilities.

Procedure: Beam Foil Spectroscopy

The measurement of this lifetime was done with the Toledo Heavy Ion Accelerator (THIA), using beam-foil spectroscopy. A schematic picture of the accelerator is shown in Appendix A. The source (powdered phosphorus) was first placed in a very thin, tube-like "oven" about four inches long. The oven was then secured next to an anode and a filament made of tungsten. A small, thin pipe perhaps a millimeter in diameter connects the phosphorous

powder to a source of argon gas. This gas provided a stable medium to carry the ionized phosphorus, akin to how water carries sodium chloride. Once ready to create an ion beam, a high voltage was applied to the source and the gas in the chamber with the source was pressurized. The small oven was then heated in order to vaporize the phosphorus and allow it to mix with the argon. As the voltage was increased to the tune of 30 kV, more electrons were emitted from the filament—colliding with the incoming gas and ionizing it in the process [6].

Ultimately, an ionized plasma developed, which was a mixture of the gaseous argon and ionized phosphorus. Its presence was immediately apparent as the current through the chamber instantly shot-up. In a few of the runs this plasma actually took quite a while to develop as it required tweaking of the gas pressure, voltage, magnetic field , as well as oven heat. Once attained, the argon/phosphorus mixture was accelerated through an electric field and deflected by the "mass selector electromagnet" in Appendix A. The magnets are adjusted to deflect only the ions of a particular mass – in the case of phosphorus approximately 31.0 amu.

Following the path in the figure into the main acceleration column, the beam's vertical and horizontal direction in the accelerator column is adjusted with a controllable electric field. Once the path is satisfactory (i.e. the beam is stable and relatively straight), the electrostatic deflection chamber sends the beam at a small fraction (<1%) of the speed of light into a thin carbon foil. Upon impact, the phosphorus ions may transfer charge and electrons become excited to higher energy levels. The magnitude of these energy levels depends on the beam's energy. The electrons then spontaneously decay to their ground states as they exit the foil.

In order to measure the lifetime of these transitions to the ground state a channeltron was used. It effectively measures the intensity of a certain wavelength of electromagnetic spectrum—in this case of the lowest intrashell transition of P (IV), 950.7 Å—and takes counts of individual photons being emitted from the transitions of the characteristic wavelength and energy.

To model the decay, the detector is moved from the foil in regular time steps, making an intensity count at each step. The result is an exponential decay of the intensity of the particular wavelength as a function of distance from the foil. This can be easily translated to be a function time by dividing all the lengths by the constant beam speed, which was 1.2 mm/ns for the 240 keV energy supply. Five such decays were measured.

Now to verify that there were no significant systematic errors in the measurement, the procedure was repeated five more times, varying the direction of the detector movement and the energy of the beam. Three runs were modeled at the same energy as before but in the "reverse" direction, where the detector was moved toward the foil, instead of away from it. This essentially checked that the detection equipment was mechanically sound. Two more runs were done, once more with the detector moving in the "forward" direction, but this time applying an energy of only 190 keV, about 25% less than the previous runs in both the forward and reverse directions. While this means a slower beam speed, and in turn more collisions with the beam-foil, the lifetime for the 950.7 Å transition should not theoretically vary from the higher energy. Since higher ionized atoms and higher excited states are created at higher energies, a lower energy is an effective way to tell whether there is blending and cascade complications (see Error section below) in the data—which can result from both excitations from the same ion P (IV) or from P (III), P (V) etc.

Data Collection

      The wavelength settings as well as dwell times for the counts of the detector were controlled by a LabVIEW VI created by Shan Ambalanth here at the University of Toledo. This program showed the real-time compilation of the decay plots and stored the numerical data in designated files. Appendix C shows the raw data of the intensity counts. This data included the distance steps from the foil, the intensity/number of counts, and the signals across the optical monitor and faraday cup.

      Using Microsoft Excel, the counts for the five primary (240 keV, forward foil) runs, the three reversed runs (240 keV), and the two lower energy runs (190 keV, forward foil) were each separately added. Then the foil positions were normalized so that the peak of the three sets of summed data corresponded to zero on the foil position. While it doesn't necessarily affect the lifetime calculation, this adjustment is physically sound—as it implies a start to the decay upon leaving the foil—and, more importantly, it allows for a better comparison of the three compiled data sets.

      The Mathematica non-linear fit function NonlinearRegress was used to fit the three sets of data to suitable two exponential curves. NonlinearRegress uses the Levenberg-Marquardt method, which computes a least-squares fit to minimize the $\chi2$ value. In general, the two exponential fits proved remarkably well in modeling the data points for all three data sets. The data and fitted-curve is shown in Figure 2(a). Figure 2(b) shows the same data, but with a semi-log plot; the two decays are very clear and meet at approximately 2 nm.

Figure 2: Intensity data for λ 950.7Å measured at 240 keV with detector moving away from foil; (a) is the normal plot with a two-exponential fit, (b) is the same plot but on vertical log scale

(a)   **Distance from foil (mm)**   (b)
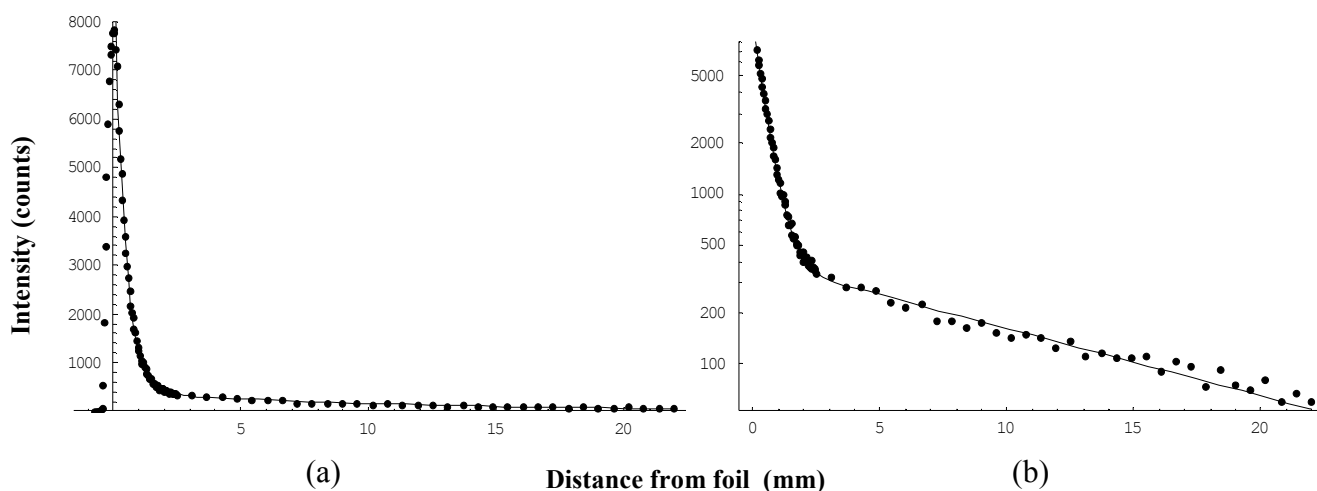
Finally, it is wise to compare the three plots visually as well as numerically. Figure 3(a) and (b) on the next page show all three fits (normal (high energy), low energy, reverse direction) on the same graph. Once again, the first shows the regular fitted plots—this time with uniform

exponential coefficients of 10—and the second plot includes the same three fits but on a semilog axis.

Figure 3: Comparison of fitted normalized plots for decay measurements at 240 keV, 190 keV and reverse decay
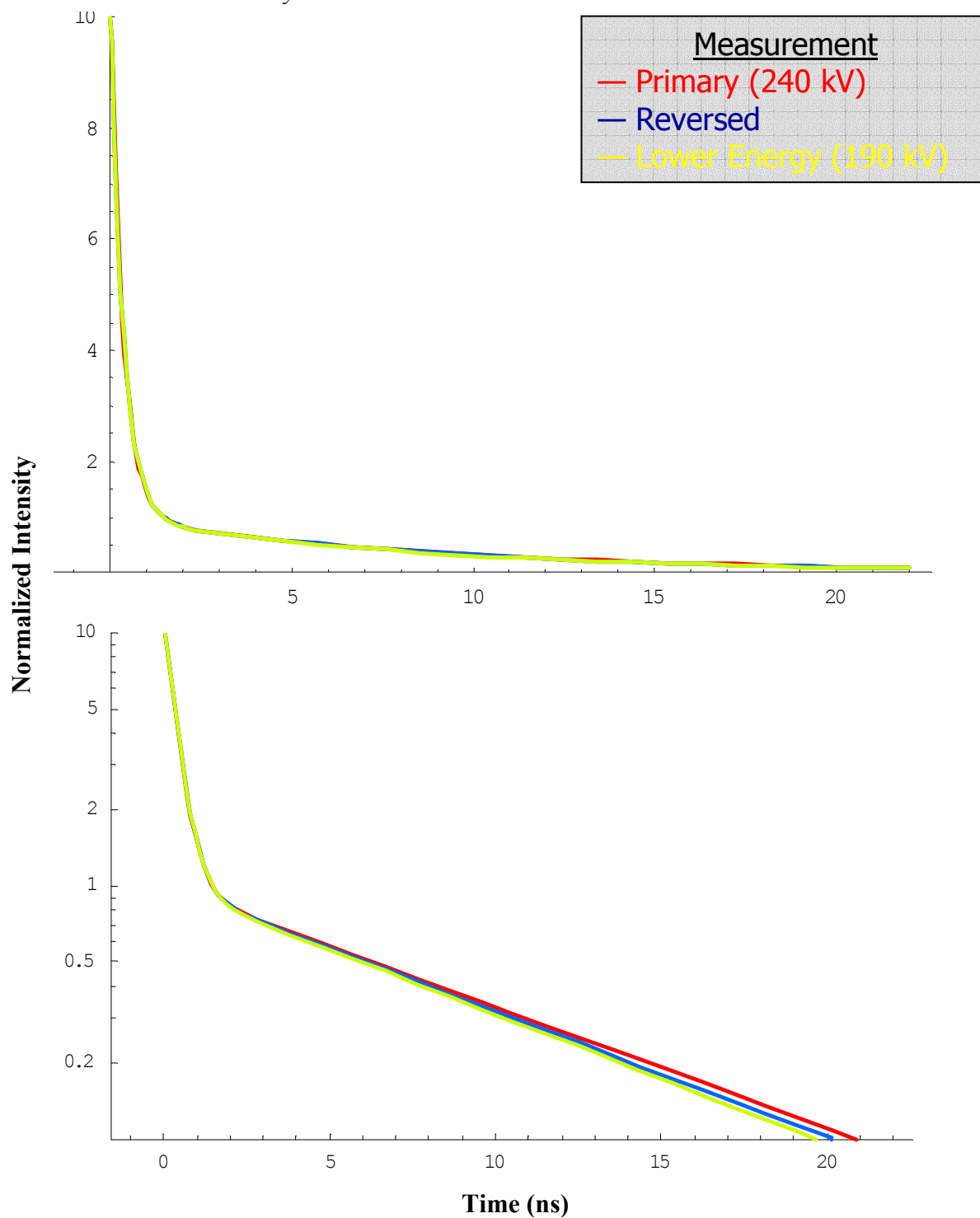
The closeness of the three fits is a strong indication that there was little systematic error in the measurements.

Results / Calculations

Table 1: Lifetime calculations for the two decays and subsequent dipole polarizability calculation with uniform 5% uncertainty in measurements

Conditions	Primary lifetime (ns)	Secondary lifetime (ns)	Dipole Polarizability (a_0^3)
Standard (5 runs)	.35 +/-.02	9.1 +/- .5	5.36
Reverse (3 runs)	.36 +/-.02	8.5 +/- .4	5.28
Low E (2 runs)	.36 +/-.02	8.8 +/- .4	5.28
Mean	.36 +/-.02	8.8 +/-.4	5.31

The results of the τ-determination from the two-exponential fits on the previous page are displayed numerically in Table 1 above. The sharp correlation of the plots is mirrored by the nearly identical measured lifetimes in the three sets of runs.

Using equations (1) and (3) we can formulate the dipole polarizability in terms of the measured lifetime by rewriting the $f - \tau$ relationship of (1) and inputing the result into (3):

$$f_{ns,np} = \frac{3a_0}{2cE_{ns,np}^2 \alpha^4 \tau} \tag{6}$$

$$\alpha_d \approx \frac{3a_0}{2cE_{ns,np}^4 \alpha^4 \tau} + \frac{(2cE_{ns,np}^2 \alpha^4 \tau)N_e - 3a_0}{4cE_{ns,np}^2 E_{ns,(n+1)p}^2 \alpha^4 \tau} \tag{7}$$

The values of all the constants and energies are displayed in Appendix A. The resulting dipole polarizability calculations are shown in Table 1.

Despite the strong agreement of the three fits and the agreement with the previous lifetime measurement of .35 ns, the resulting dipole polarizability is worryingly smaller than the measured value of 6.31 a_0^3 by Magnusson and Zetterberg. Possibilities for this discrepancy are explored in the next section.

However, perhaps the most glaring indication of the error in the measurement can be seen in the change of the isoelectronic plot of $1/(Z-C)$ vs Z^2S, where Z is the atomic number, S is the line strength, and C is an arbitrary constant—adjusted to linearize the points. Figure 4 on the next page shows how a .35 ns lifetime measurement disrupts the linearity of the plot, while the previous α_d measurement supports the linearity very well.

Figure 4: Comparison of Isolectronic plot using the previous α_d measurement (a) to the new plot based on new the P (IV) lifetime (b)

(a)   (b)
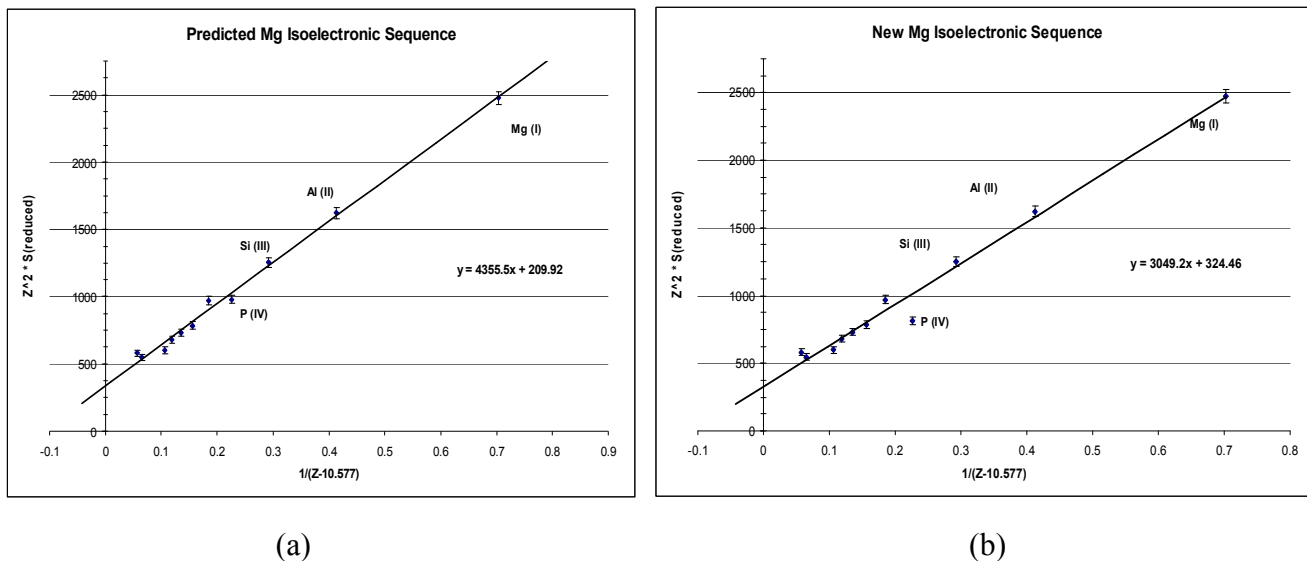
Error Analysis

There are several places to look at for the source of the error in the lifetime measurement. There may have been technical problems with the intensity measuring device (channeltron). Also, the fitting data selected or the fitting method used, Mathematica's NonlinearRegress, may be flawed. More likely, however, the problem was not so much in the accuracy of the data or in its manipulation, as in its interpretation. For, one of the limitations of beam foil spectroscopy (BFS)—and other non-selective lifetime determination techniques—is its very "non-selectivity." The fact that BFS gives access to virtually all transitions and excites all levels is a double-edged sword. On the one hand, you can look at transitions very difficult to see through non-selective means; on the other hand, there is the potential for blends and cascades to interfere with the lifetime you are interested in measuring. Interference from cascades from higher levels into the 3s3p level of P (IV) may very well account for the higher-than-expected lifetime determination. Still, all sources of error must be considered.

Beam stability

The first place to check was the beam stability. Of course one way to check that it's stable is to monitor the voltage coming through the acceleration chamber. However, what is more important is the stability of the beam up and around the actual foil and detector. There are two pieces of equipment for this purpose: the faraday cup and the optical monitor. The former detects the ions (and thus the current) that come out of the foil, while the latter detects the actual intensity of the light with a photomultiplier tube. While the technical aspects are a bit

complicated, the basic idea is that the signals of both of these detectors to be stable—as close to constant as possible. The standard way to check this is to normalize the signals of both detectors and then take their ratio; the closer the ratio is to one, the more stable the beam and more reliable the data. In general, a ratio between 1 and 1.2 is considered adequate. Figure 5 shows two of the normalized signal comparisons of the faraday cup and optical monitor. Green is the faraday cup, blue the optical monitor, and red is the ratio optical monitor/faraday cup.

Figure 5: Comparison of Beam stability for two runs at 240 keV, forward direction
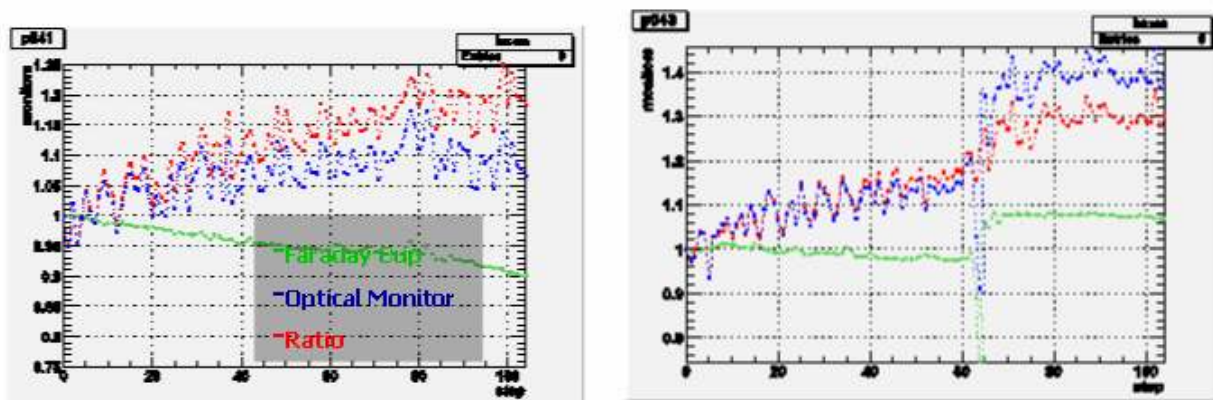
Despite the general increasing trend of the ratio in the run at the left, the ratio stayed below 1.2 for most of the run and the data is considered reliable. The run shown at the right, however, should be suspect to scrutiny given the sudden fall and jump in the signals and the ratio. However, in general the ratios for the plot were in the general safe range of 1 to 1.2 and thus it is unlikely that beam fluctuations could account for the high lifetime measurement.

Fitting and Mathematica

The data region picked to be fitted must be picked a few points *after* the start of the decay, after the peak in the curve. It is only after those few initial counts at the peak that the true exponential decay begins. The best way to pick exactly where to begin the region is by checking to find the two points that have the greatest difference from each other and after which the successive differences are all smaller. This ensures that you are looking at the decay and not at the effects of beam foil collisions. Given the remarkable visual fit to the data points shown in Figure 2(a) and the other curves, this was not a problem.

While certainly adding to the total uncertainty of the lifetime determination, the Mathematica method used is even lesser likely to account for the high lifetime. This is perhaps best seen by the superb two-exponential fits for all three data sets shown in Figure 3. However, Mathematica itself can calculate the deviation of the data from the fit. In particular, the confidence interval of the data—the interval where there is a 95% chance of the data to fall—was calculated for the nonlinear regressions for the three fits in the table on the next page.

Table 2: Confidence intervals for Mathematica's nonlinear fits to decay data for P (IV)

Type	Confidence Interval (ns)
240 keV, forward detector	(.349,.357)
240 keV, reverse detector	(.354,.364)
190 kev, forward detector	(.352,.365)

Given the general agreement of the confidence regions and the strong correlation between the curves and the data points, uncertainty in the fitting method can be discounted.

Cascades and Blending

The final, and most important consideration to make is of the cascades to the 3s3p $^1P_1^o$ level and the blending potential from other charged states of phosphorus. Figure 6 shows four different cascades to the energy state that we are interested in. And two of them, 3s4s $^1S_0$ and 3s^{2}S$_0$, have lifetimes very close to the lowest resonance λ 950.7 Å that we're interested in. Thus, the decay curve that was measured likely included the decays of all these higher energy states. Their contributions depend on their transition probablities, and as they are high for at least two of them, the ~.36 ns measurement of the experiment more than likely includes these higher energy states.

Figure 6 : lifetimes and wavelengths for P(IV) cascades [7]
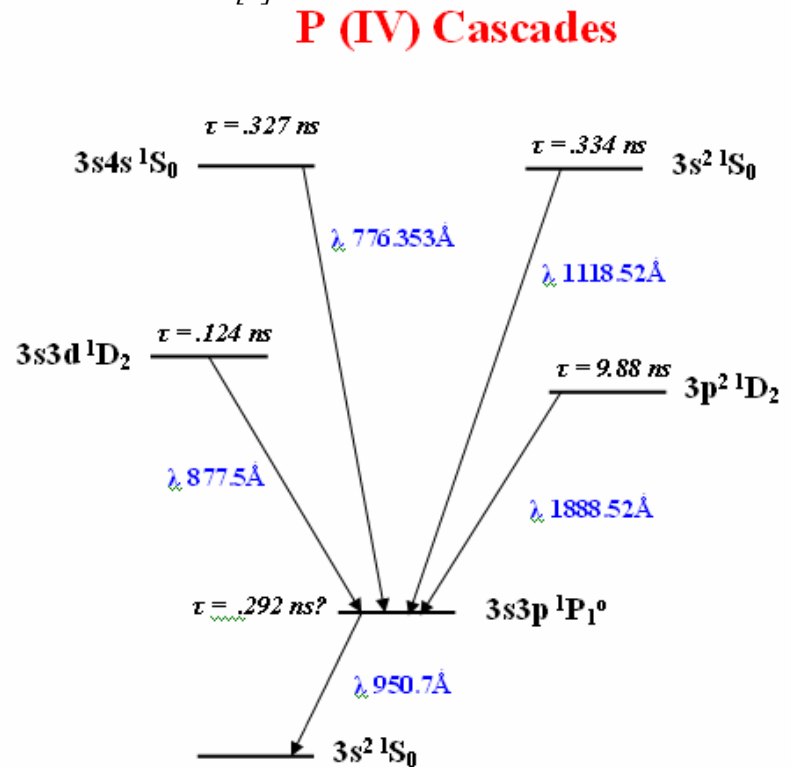
So, the intensity measured is really the sum of all the exponential decays coming into the upper level:

$$I = \sum_i c_i e^{-t/\tau_i} \tag{8}$$

Notice the long decay from 3p2^{1}D$_2$. This accounts for the long tail in the two-exponential fits, and nearly matches the ~ 9.0 ns determined from the fit for the secondary decay.

Now, it may seem that the possibility of all these cascades contradicts the precise decay fit attained with Mathematica; afterall the two-exponential fit was visually remarkably accurate.

Yet, as these cascades have very short lifetimes, their contribution may be small in terms of the visual fit. Even a sophisticated computer fitting method would be unable to decouple the other exponentials. However, through a technique known as ANDC, invented by Curtis [2], the multiple exponential decays can be decoupled by empirical measurements of the different contributing cascades.

In fact, the ANDC method could have been used to decouple all the cascades and scale down the overly high lifetime determination were it not for the additional complication of blending. Blending essentially occurs when transitions—usually in different charged ions of the same atom—have the same or very close characteristic wavelength. If the wavelengths of the transitions are closer than the range of the spectrometer (channeltron in our case), it can be nearly impossible to distinguish between the two decays. And this is exactly the case for the $3s^2{}^1S_0$ transition at $\lambda 1188$ Å. It turns out that the lowest ground state transition for *P (V)*, has a wavelength of difference less than an Angstrom. Without the ability to resolve the $3s^2{}^1S_0$ in P(IV) from the decay from the $3p^1P_1{}^o$ of P(V), decoupling the exponentials is hopeless.

Thus, the higher-than-expected lifetime determination is more than likely of these cascades falling from higher energy states. Though usually solvable, this problem is confounded by the blending from the P (V) ion. This demonstrates one of the pitfalls of beam foil spectroscopy, where unwanted interference can occur from differently ionized states.

Conclusion and Prospects

While the lifetime determination gave a value too high, there is still a potential for resolving the lifetime from the cascades. For, even though energies of 240 and 190 keV seem to cause the blending to occur—given the near identical lifetime determinations for the different energies—an even lower enough energy can eliminate it.

If the beam is run at a lower energy, it will collide with the foil at a slower speed. And if that speed is small enough so that only ions of the magnitude of P (IV) (and no higher) are created, the blending from P(V) can be removed. The ANDC method can then be used to decouple the four cascades into the $3s3p^1P_1{}^o$ level.

Unfortunately, there is a tradeoff with running at lower energies. For as the speed of the beam is decreased there is a longer dwell time of the ions in the foil and more collisions. The result is a shortened foil life. Additionally, a lower energy means less excitation and weaker intensity of the beam at any given wavelength. A lower intensity means less counts will be made and thus there will be more uncertainty in the measurements.

The most effective method will be to gradually shift the energy down until there is a noticeable difference in the decay curve at $\lambda 1118$ Å. This will ensure that the energy is as high as it can possibly be in order to remove the blend from P (V), and do minimum damage to the foil.

But whether or not the lifetime can be improved to be compatible with the isoelectronic plots of Figure 4 and the previous α_d measurement, the P(IV) ion truly revealed the power of this two way relationship between transition lifetimes and dipole polarizability for atoms with the outer configurations ns^2. While it would be nice to have a confirmation of the predictions of the isoelectronic sequence and resolve the previously measured conflicting lifetimes, this is not

essential. Even for ions where one of these quantities is difficult to measure or plagued by unlucky circumstances (such as blending) the other one can be measured to get both pieces of information. And even if neither quantity can be measured for a certain complex system, interpolation and extrapolation can always be invoked in the linear isoelectronic plots derived from just a few precise measurements of *either* τ or α_d.

The potential of such mutually reinforcing relationships is powerful in extracting information about inner electrons. As of right now, it has been successfully applied only for the atomic systems with ns or ns^2 configurations. It would be natural to try it for other systems. However, dipole polarizability and transition lifetimes are just one pair of compatible quantities. The broader prospect for future research is to explore *similar* relationships between other empirical quantities in atomic systems of other configurations.

Acknowledgements

References

[1] L. J. Curtis. "Determination of lifetimes and nonadiabatic correlations from measured dipole polarizabilities," J. Phys. B: At. Mol. Opt. Phys. **40**, 3173-3180 (2007).

[2] L. J. Curtis. *Atomic Structures and Lifetimes: A Conceptual Approach*. Cambridge University Press: Cambridge, 2003. 131-137, 200-202

[3] Curtis L J, Martinson I and Buchta R 1971 *Phys. Scr.* **3** 197-202

[4] Livingston A E, Kernahan J A, Irwin D J G and Pinnington E H 1975 *Phys. Scr.* **12** 223-229

[5] Magnusson C E and Zetterberg P O 1977 *Phys. Scr.* **15** 237-250

[6] R. R. Haar, D. J. Beideck, L. J. Curtis, T. J. Kvale, A. Sen, R. M. Schectman and H. Stevens, "The Toledo Heavy Ion Accelerator," Nucl.Instr. and Meth. in Phys. Res. B **79**, 746-8 (1993).

[7] G. Tachiev and C. Froese Fischer, Method: MCHF (ab initio), 2002

Appendix

A. The Toledo Heavy Ion Accelerator
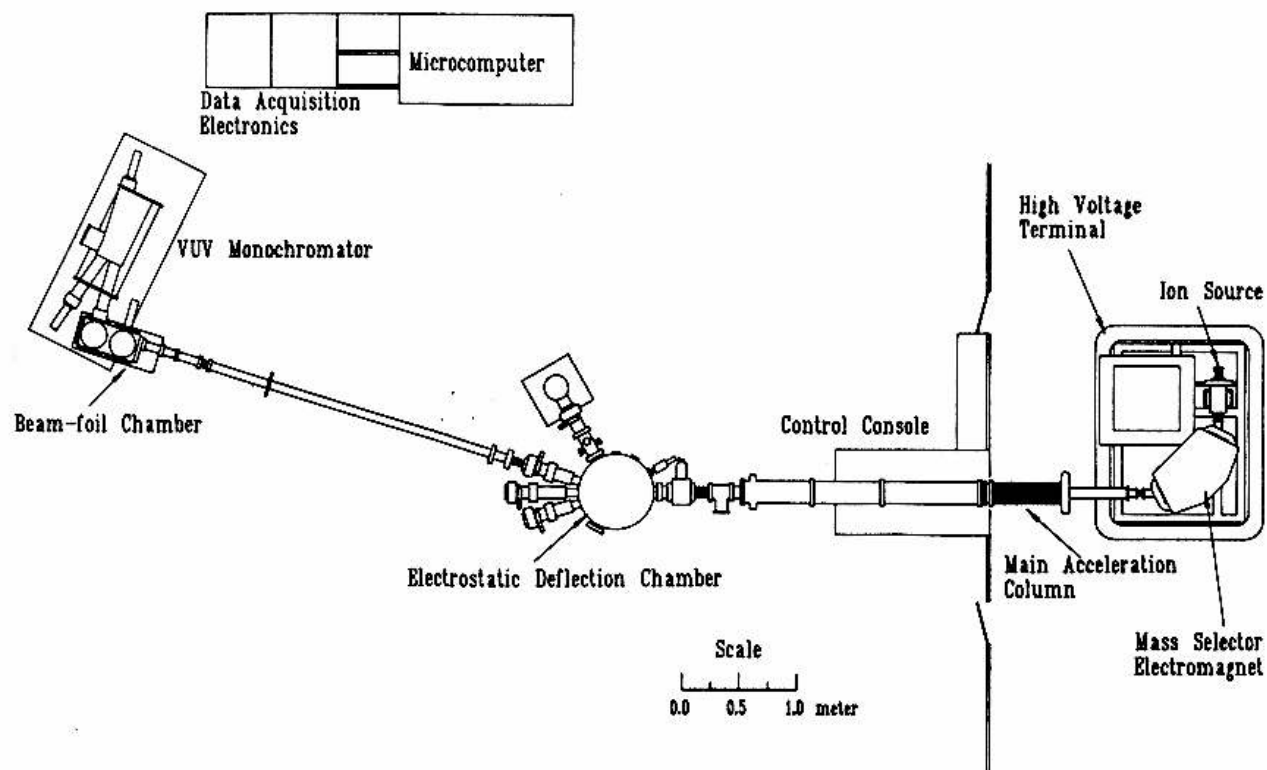
Fig. 1. A schematic of the general layout of the Toledo heavy ion accelerator facility, THIA.

B. Important Constants and Energies

Quantity	Value
Bohr Radius, a_0	$52.918 * 10\wedge\text{-}12$ m
Speed of light, c	$299792458/10^9$ m/ns
Fine structure constant, α	$1/137.035999976$
P (IV) Valence e$^-$ + core contribution, N_e	2.1
P(IV) $E_{3s,3p}$	.479283 Hartrees
P(IV) $E_{3s,4p}$	1.173360 Hartrees

C. Raw Decay Data: Intensity counts of the channeltron for 10 runs, (5 at 240 keV, forward moving), (3 at 240 keV, reverse moving), (2 at 190 keV, forward moving)

foil distance	HighE 1	HighE 2	HighE 3	HighE 4	HighE 5	Rev 1	Rev 2	Rev 3	LowE 1	LowE 2
-1.7	5	2	2	0	0	12	16	11	1	2
-1.655	4	1	1	1	2	14	13	13	2	0
-1.61	2	1	0	0	2	10	21	9	0	4
-1.565	1	1	0	1	0	14	11	13	1	5
-1.52	5	1	0	0	1	18	12	19	0	1
-1.475	3	2	3	2	2	16	14	17	2	4
-1.43	23	5	37	1	2	11	16	21	6	2
-1.385	204	28	228	43	29	14	22	19	14	4
-1.34	555	260	524	228	247	17	6	25	190	9
-1.295	926	641	810	446	584	17	21	17	628	75
-1.25	1301	934	979	742	858	15	23	23	1215	458
-1.205	1461	1296	1143	889	1110	17	25	32	1796	1121
-1.16	1708	1500	1266	1026	1283	17	27	20	2245	1767
-1.115	1724	1740	1323	1176	1355	20	27	16	2462	2308
-1.07	1789	1769	1372	1151	1407	25	26	31	2696	2630
-1.025	1771	1859	1458	1203	1488	23	21	25	2620	2907
-0.98	1848	1896	1429	1205	1462	21	19	45	2658	3066
-0.935	1787	1824	1386	1273	1486	27	27	30	2512	3067
-0.89	1699	1801	1279	1215	1455	25	19	29	2594	3054
-0.845	1558	1785	1143	1168	1448	21	24	54	2471	2946
-0.8	1410	1557	985	1055	1297	30	27	39	2324	2803
-0.755	1285	1465	884	1003	1147	32	38	42	2139	2841
-0.71	1112	1276	884	860	1046	18	46	40	2065	2460
-0.665	1091	1245	793	783	969	38	44	53	1871	2252
-0.62	963	1120	687	706	867	44	45	41	1657	2000
-0.576	853	959	649	650	826	36	34	55	1475	1856
-0.531	823	891	550	602	718	45	45	46	1380	1729
-0.486	725	851	520	516	644	49	55	62	1200	1477
-0.441	693	750	474	491	583	42	63	53	1036	1335
-0.396	621	660	428	473	569	43	54	61	943	1227
-0.351	542	642	401	384	494	47	68	71	836	1127
-0.306	446	543	322	398	467	61	56	68	792	993
-0.261	442	523	315	319	441	53	77	66	657	845
-0.216	396	508	296	342	382	64	72	95	600	775
-0.171	386	423	292	268	339	55	89	86	540	675
-0.126	350	411	270	272	326	63	81	96	471	674
-0.081	301	361	240	249	293	76	78	72	444	579
-0.036	288	336	214	207	269	72	78	81	427	533
0.009	284	312	169	224	245	88	96	95	365	549
0.054	270	274	204	181	236	77	74	82	363	480
0.099	232	248	182	159	216	61	92	72	355	426
0.144	207	243	175	172	191	78	85	99	327	385
0.189	244	239	157	150	214	80	96	103	307	364
0.234	204	216	153	158	187	70	92	96	280	356
0.279	185	233	146	145	168	75	98	108	265	339

0.324	156	199	117	130	166	77	74	98	239	325
0.369	168	208	105	114	156	86	95	109	215	279
0.414	156	175	96	117	122	58	89	97	239	282
0.459	159	186	90	84	141	82	103	116	199	221
0.504	128	196	105	110	140	87	104	112	199	245
0.549	129	136	96	88	130	81	93	91	171	235
0.594	109	125	101	98	121	97	107	87	171	201
0.639	116	150	86	104	107	107	106	122	156	219
0.684	110	126	100	66	109	99	106	117	163	172
0.729	115	127	93	88	97	90	123	133	176	174
0.774	116	138	85	85	82	80	119	123	145	211
0.819	86	112	75	88	83	83	137	139	138	201
0.864	96	115	93	60	92	114	132	142	129	168
0.909	99	96	88	77	93	93	137	160	126	160
0.954	82	116	88	73	98	120	159	156	122	169
0.999	78	108	69	56	92	123	137	184	120	173
1.044	85	112	57	61	105	124	159	182	125	151
1.089	90	106	92	65	79	151	183	177	127	159
1.134	103	96	76	61	71	167	181	195	105	138
1.179	86	99	69	53	79	166	159	204	111	127
1.224	83	81	57	71	80	143	217	221	123	142
1.269	85	99	66	71	90	172	194	215	116	135
1.314	74	104	49	73	70	170	205	258	108	135
1.359	82	90	68	64	71	200	265	271	117	134
1.404	75	103	62	54	74	209	255	265	110	134
1.449	85	72	69	57	76	193	261	266	101	134
1.494	72	70	80	45	73	236	286	307	103	136
2.08	78	75	59	43	69	253	324	323	101	129
2.67	54	66	49	53	61	275	361	360	107	106
3.26	67	51	63	55	50	298	364	410	81	87
3.85	71	69	45	40	47	304	436	443	90	89
4.44	54	49	40	38	53	367	445	502	66	82
5.03	51	45	37	41	44	403	469	508	68	82
5.62	54	38	50	45	41	426	560	578	56	76
6.21	43	49	29	30	29	490	599	589	63	55
6.8	42	41	27	38	32	492	697	681	41	59
7.39	45	39	25	21	34	571	726	723	59	52
7.98	36	40	33	32	34	584	791	806	43	65
8.57	34	41	27	22	31	707	779	907	44	57
9.16	27	31	27	33	25	740	940	956	47	61
9.75	31	31	28	21	38	886	966	1041	41	46
10.34	30	42	16	30	25	877	1090	1191	38	53
10.93	22	37	19	19	28	969	1212	1318	35	53
11.52	28	26	27	23	33	1040	1389	1404	27	30
12.11	25	25	20	19	22	1115	1426	1464	35	37
12.7	21	24	20	28	23	1246	1513	1573	26	24
13.29	21	20	22	20	25	1242	1593	1641	28	22
13.88	27	19	25	22	15	1280	1534	1655	24	32
14.47	18	36	17	16	24	1293	1552	1663	29	32
15.06	24	21	18	12	15	1154	1358	1568	26	27

15.65	24	28	11	22	20	1175	1341	1460	21	39
16.24	22	26	17	15	18	1065	1280	1394	23	28
16.83	21	13	14	10	16	997	1146	1304	15	22
17.42	14	26	21	15	17	933	932	1070	22	24
18.01	15	12	16	19	14	758	774	873	17	18
18.6	21	13	9	15	13	579	424	594	12	24
19.19	15	14	14	19	19	313	168	283	21	21
19.78	23	10	9	11	7	80	15	52	13	12
20.37	20	17	7	11	12	14	0	6	9	13
20.96	15	14	8	8	15	6	1	0	14	9